FAILURE IN PLAIN AND REINFORCED CONCRETE—AN ANALYSIS OF CRACK WIDTH AND CRACK SPACING

L. J. SLUYS

Delft University of Technology, Department of Civil Engineering, P.O. Box 5048,
2600 GA Delft, The Netherlands

and

R. de BORST

Delft University of Technology, Department of Civil Engineering/Eindhoven University
of Technology, Department of Mechanical Engineering, P.O. Box 5048, 2600 GA Delft,
The Netherlands

Abstract—The proper prediction of crack widths in plain concrete and the spacing of primary cracks in reinforced concrete are the subject of this paper. Attention is focused on the influence of the crack concept. A comparison has been made between the standard crack model, the crack model with the fracture energy as a separate parameter, the rate-dependent crack model and the gradient crack model. It is shown that for reinforced concrete, use of one of the first two models results in a random location of primary cracks and consequently in a random value for the crack spacing. The effect of the inclusion of a length scale parameter in the latter two models has been determined with respect to the crack width in plain concrete and the crack spacing in reinforced concrete. Furthermore, attention is paid to the crucial role of the bond–slip characteristic in predicting crack spacing in reinforced elements. Copyright © 1996 Elsevier Science Ltd.

1. INTRODUCTION

In this paper we focus on the proper prediction of the width of cracks in plain concrete and the width and spacing of primary cracks in reinforced concrete. The influence of the crack concept on these quantities and, more specifically, the introduction of a length scale in the crack concept will be investigated. The length scale parameter not only sets the width of a single crack, but in cases where redistribution of stresses and multiple cracking is possible, as for instance in reinforced concrete, it also heavily influences the spacing between cracks.

If we use a standard crack model for the description of concrete a mesh sensitivity occurs during the formation of a single crack and also with respect to the pattern of primary cracks in reinforced concrete. The width of a single crack and the spacing between the primary cracks is affected by the discretization, i.e. a smaller element size results in a smaller crack width and in random distances between cracks. For dynamic calculations the value for the crack spacing is not only dependent on the spatial discretization but also on the discretization in time. On the other hand, when a pattern of cracks has developed fully the behavior is mainly determined by the steel and no additional spurious mesh size effects occur. Enhancing the crack model by including the fracture energy as a separate material parameter does not solve the problem for reinforced concrete, since the amount of energy that is released by a fully developed pattern of primary cracks is determined by firstly the energy consumption of a single crack and secondly the crack spacing. It will be shown that this latter quantity is not predicted correctly with a so-called fracture energy-type crack model.

To remedy this improper behavior the standard crack model can be enriched by adding higher-order terms, either spatially or in the time domain. Alternatively, discontinuities like cracks can directly be incorporated into the element concept, e.g. along the lines proposed by Simo (Simo *et al.*, 1993; Simo, 1994). Higher-order models introduce a length scale

parameter that reflects the inhomogeneous micro-structure of the material. This parameter sets the size of the fracture process zone. This will be illustrated for plain concrete using a strain-rate dependent crack model for a double-notched specimen problem under impact loading. In reinforced concrete structures the introduction of a length scale through higher-order strain-rate or strain-gradient terms determines the failure mode and is proportional to the spacing of the primary cracks. Use of the gradient model therefore removes the mesh dependence in the primary crack spacing and a comparison with experimentally measured values for the crack spacing may provide a physically realistic estimation of the length scale parameter. The proper modeling of the bond–slip behavior is also of crucial importance. An analysis has been carried out on a bar with one reinforcing bar loaded at both sides by a dynamic load. The dynamic case for this problem is easier to perform computationally. The evolution of the primary crack pattern follows the stress wave and, depending on the crack formulation, primary cracks occur at more or less regular distances. In statics, on the other hand, the first primary cracks occur at imperfect locations and other cracks form at intermediate points which gives a value for the crack spacing. So, in dynamic computations no imperfections have to be included because the non-uniform solution is driven by the stress wave. The evolution of primary cracks is different from the static case, but the resulting value for the crack spacing is of the same order, except for a negligible rate effect.

2. GEOMETRICAL MODELING OF REINFORCED CONCRETE

A number of approaches for the finite element modeling of reinforced concrete can be distinguished. If the micro-behavior in the vicinity of the reinforcing bar is of particular interest a modeling of the reinforcing bar with ribs that provide the mechanical interlock is required. By using such a computational model next to the primary or dominant cracks, secondary transverse cracks, longitudinal cracks and crushing in compressive zones close to the ribs can be analyzed (Rots, 1988). This approach is essential for a better understanding of the bond–slip behavior between the concrete and the steel. However, for analyses of reinforced concrete members the above approach is too complicated since it includes all possible mechanisms. Depending on the distribution of the reinforcement, two approaches can be used. When the reinforcement is concentrated in a few dominant reinforcing bars the traction–slip behavior can be lumped into interfaces. The width and spacing of the primary cracks can be studied with this type of modeling. Alternatively, when the concrete is densely reinforced not every reinforcing bar can be modeled separately and an embedded formulation is commonly used to model the primary cracks. Tension-stiffening then accounts for the bond characteristics, but a true slip behavior between the concrete and the steel cannot be modeled (Feenstra, 1993). In the analyses it will be demonstrated that this slip behavior dominates the spacing of the primary cracks.

In this paper we focus on the proper prediction of the width and the spacing of primary cracks in reinforced concrete. A level of modeling is adopted in which the traction–slip behavior is explicitly taken into account via interface elements. In this fashion the influence of the material characteristics for concrete, bond–slip and steel on the crack spacing can be analyzed. An example of the finite element idealization of the composite material is shown in Fig. 1, in which the steel reinforcement bars have been modeled with three-noded truss elements, and in which six-noded interface elements have been introduced for the modeling of the bond–slip behavior between the concrete and the reinforcement. The width i of the interface element (Fig. 1) is equal to zero, while the thickness of the interface element is equal to the periphery of the reinforcement bar. It is noted that such a model gives a small overestimation of the cross-sectional area because the reinforcement is modeled in addition to the beam. For this reason the density and the stiffness of the beam are slightly larger.

3. MATERIAL MODELING OF PLAIN AND REINFORCED CONCRETE

The crack concepts that will be used for plain and reinforced concrete will be discussed now. We used a smeared model in which the crack is conceived to be a continuum which permits a description in terms of stress–strain relations. Four different concepts have been
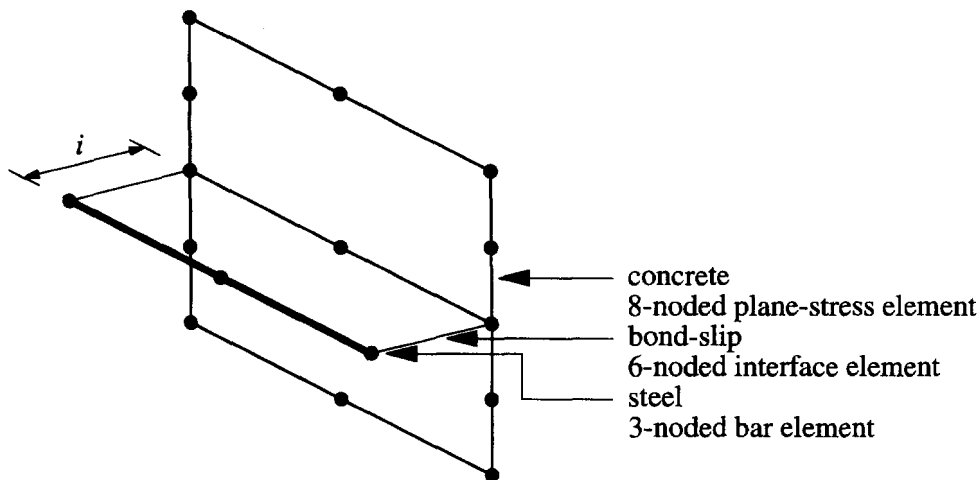
Fig. 1. Finite element idealization of reinforced element.

analyzed, namely the standard crack concept, the G_f-type crack concept, the strain-rate dependent crack concept and the strain-gradient dependent crack concept. Additionally, for reinforced concrete the constitutive relation for the steel is defined and the interactive forces between the concrete and the steel bars are determined via a bond–slip relation, which is the constitutive equation of the interface element.

Concrete : the standard crack model

In the standard formulation for cracking we use a decomposition of total strain ε into an elastic strain ε_e and a crack strain ε_{cr}. In a major principal stress direction a stress degradation takes place according to

$$\sigma = f_t + h\varepsilon_{cr}, \tag{1}$$

where σ denotes stress, f_t is the initial tensile strength and h is a constant negative softening modulus. The use of a standard model for cracking results in an ill-posed problem, e.g. under dynamic loading conditions each wave has an imaginary wave speed. As a consequence, a continuum discretized in finite elements always shows a crack zone which is only one element wide (*mesh sensitivity problem*). It appears that this solution for the cracked zone belongs to a wave with a speed equal to zero (stationary wave) and a width (wave length) equal to the finite element size (Sluys *et al.*, 1995). For linear elements this is demonstrated in Fig. 2, in which in the top left figure the solution for the discretized continuum is the stationary wave ($c = 0$ m s^{-1}) with wave length equal to the element size d. This constant strain element cannot reproduce the harmonic strain distribution belonging to the corresponding wave in the continuum, which causes the difference between the continuum and the discretized medium in the top left figure. In the standard continuum model a length scale is lacking which sets the width of the fracture process zone and gives information on the inhomogeneous micro-structure of the concrete. In the discretized standard continuum this length scale is thus set by the size of the finite elements. This is also the case for reinforced concrete in which the spacing between the primary cracks is affected by the mesh size as well. A smaller mesh size implies a faster degradation of stress and consequently a second primary crack will occur sooner and at a shorter distance than the first crack.

Concrete : the G_f-type crack model

As an intermediate solution between using the standard crack model and adding higher-order terms a number of authors (Pietruszczak and Mróz, 1981; Bažant and Oh, 1983; Willam, 1984) have proposed to regard the area under the softening curve as a material parameter, namely the fracture energy.
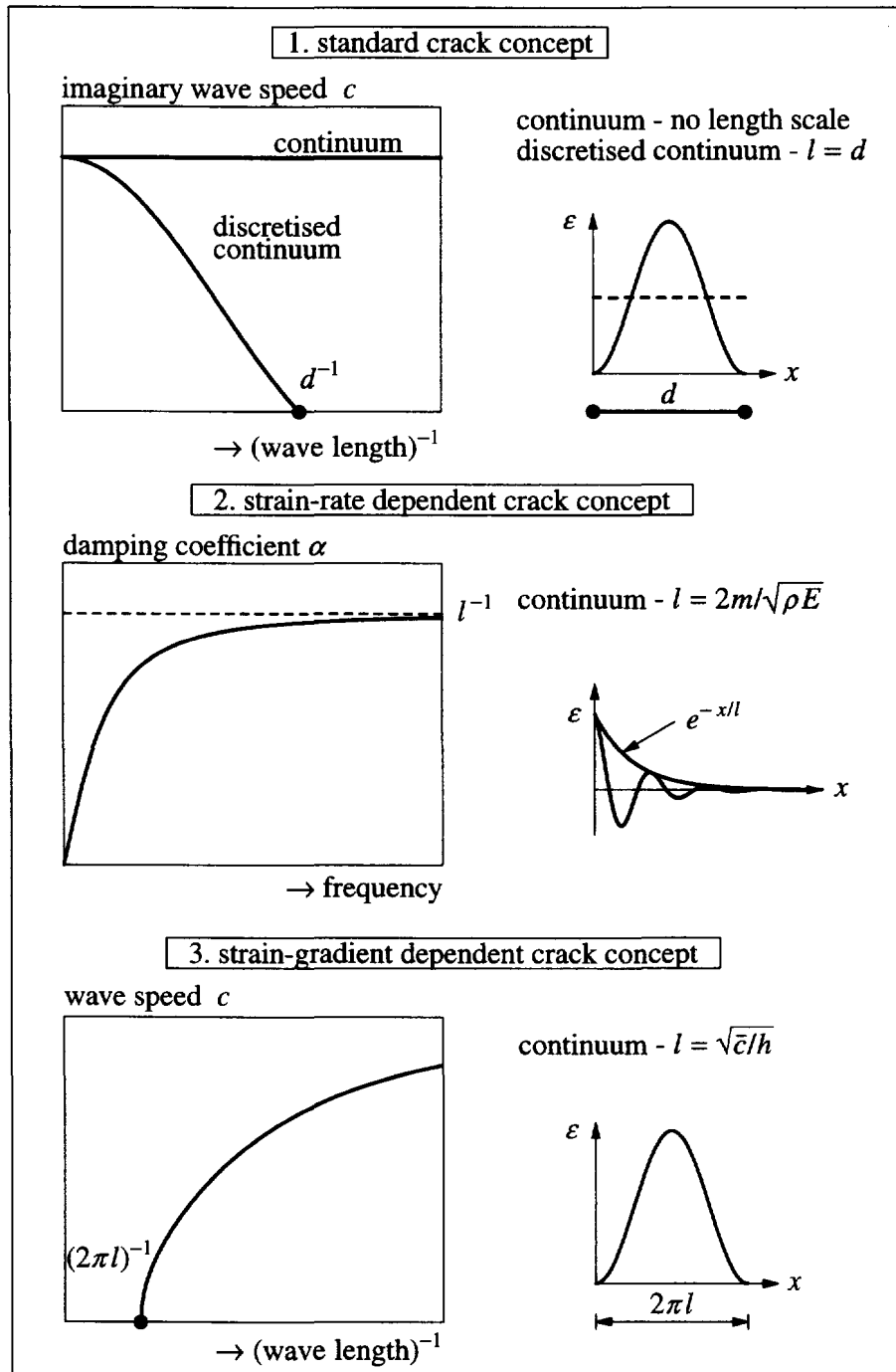
Fig. 2. Overview of length scale effects in (1) the standard concept, (2) the rate-dependent concept and (3) the gradient-dependent concept.

$$G_f = \int \sigma \, du = \int \sigma \varepsilon \, ds, \tag{2}$$

in which $0 < s < w$ with w the width of the localization zone. The fracture energy must be released over an equivalent length which, for a standard model, should correspond to a representative dimension of the mesh size. In this fashion the slope of the strain-softening diagram becomes a function of the finite element size. When we prescribe the fracture energy G_f as an additional material parameter the global load–displacement response can become insensitive to the discretization. However, locally nothing has altered and localization still takes place in one row of elements. This is logical, since the change of

character of the partial differential equations occurs locally, even though the energy that is dissipated remains constant by adapting the softening modulus to the element size. For numerical simulations this implies for instance that severe convergence problems are usually encountered if the mesh is refined. Also, the frequently reported observation still holds that the localization zones are biased by the discretization and tend to propogate along the mesh lines (Larsson, 1990; Sluys, 1992). Also, for reinforced elements the energy released in a single primary crack can be made mesh-objective in this way, but the spacing between the primary cracks still depends on the finite element configuration.

Concrete: the rate-dependent crack model

From a physical point of view the introduction of rate dependence is perhaps the most natural way to regularize ill-posed initial value problems which arise because of the introduction of damage or frictional effects (Wu and Freund, 1984; Needleman, 1988; Loret and Prévost, 1990; Sluys, 1992). Here we adopt a simple, linear rate-dependent smeared crack model as developed by Sluys (Sluys and de Borst, 1992; Sluys, 1992). In it, the major principal stress degrades according to

$$\sigma = f_t + h\varepsilon_{cr} + m\frac{\partial\varepsilon_{cr}}{\partial t}, \tag{3}$$

with ε_{cr} the crack strain, h the softening modulus and m the viscosity. This model complies with the experimental findings that the tensile strength increases under dynamic loading (Zielinski, 1982; Körmeling, 1986). From an analysis of dispersive waves it can be demonstrated that each wave in a rate-dependent cracked material has a real wave speed and each wave is attenuated in the spatial domain according to a damping coefficient (Sluys, 1992). In Fig. 2 the damping coefficient α is plotted as a function of the frequency. It is observed that for smaller wavelengths (higher frequencies) the damping coefficient becomes a constant. This constant amount of spatial damping is dependent on the viscosity of the material and is a measure for the length scale parameter (Sluys, 1992):

$$l = \frac{2m}{\sqrt{\rho E}}. \tag{4}$$

A strain profile occurs in the cracked zone that is exponentially shaped as shown in Fig. 2. For this model the rate boundary value problem remains well-posed and a length scale parameter is introduced, which ensures the removal of spurious mesh dependence.

Concrete: the gradient crack model

A second model that can be used for the concrete to regularize the ill-posed problem is the strain-gradient dependent crack model (Aifantis, 1984; Lasry and Belytschko, 1988; Mühlhaus and Aifantis, 1991; de Borst and Mühlhaus, 1992; Sluys, 1992; Pamin, 1994). Higher-order strain gradients are introduced which represent nonlocal interactions at a micro-structural level of the concrete. The model is formulated within a Rankine plasticity framework. An expression in one spatial direction reads

$$\sigma = f_t + h\varepsilon_{cr} + \bar{c}\frac{\partial^2\varepsilon_{cr}}{\partial x^2}, \tag{5}$$

with $\bar{c}$ a gradient parameter which can be regarded as a measure for the interaction length of micro-structural defects. A strain-gradient dependent continuum can only transmit waves with wave lengths smaller than a critical value. This critical value of the wave length belongs to a stationary wave (wave speed equal to zero) with a wave length which is determined by the length scale parameter of the model (cf. de Borst and Mühlhaus, 1992).

$$l = \sqrt{\frac{\bar{c}}{h}}.$$

(6)

The stationary wave with the maximum wavelength that is transmitted by the strain-gradient dependent continuum is represented by the point of intersection in the bottom left plot in Fig. 2. The wavelength is equal to $2\,\pi l$ which is the solution for the process zone of one primary crack (see Sluys et al., 1995). Mesh sensitivity is removed and the length scale parameter introduced in the model is a measure for the crack width and the crack spacing, as will be demonstrated in Section 5.

Steel reinforcement

For the steel bars a simple elastic–perfectly plastic relation has been used. In the analysis described in Section 5 the response of the steel bar remains elastic, which drives the redistribution of stresses and the occurrence of multiple cracking.

Bond–slip

Experimental data for a normal bond component are scarce and cannot be transformed into a constitutive law (Rots, 1988). Therefore, the interface normal behavior and the shear–normal coupling are not incorporated and the constitutive equation for the interface element reduces to a shear traction–slip (τ–δ) relation. This slip behavior between reinforcement and concrete has been modeled using the relation of Dörr (1980):

$$\tau = a[5.0(\delta/\delta_0) - 4.5(\delta/\delta_0)^2 + 1.4(\delta/\delta_0)^3] \quad \text{if } 0 < \delta < \delta_0$$

(7)

$$\tau = 1.9a \quad \text{if } \delta > \delta_0,$$

(8)

in which a is a constant which is taken equal to the tensile strength f_t and δ_0 is the deformation at which perfect slip occurs, which is usually taken equal to 0.06 mm.

4. PLAIN CONCRETE—PREDICTION OF CRACK WIDTH

In the Stevin Laboratory of Delft University of Technology impact direct tension tests have been carried out on double-notched, prismatic concrete specimens (Fig. 3). A specimen with notches makes it possible to predetermine the failure zone and to measure the deformation inside as well as outside the fracture zone. The tests have been performed with a Split–Hopkinson bar apparatus by Weerheijm (1992). The specimen is kept between an upper bar (6.7 m) and a lower bar (3.5 m) and the tensile pulse is applied at the bottom of the experimental set-up. The main observations that have been reported are the ultimate strength and the deformations inside and outside the fracture zone. The loading rate has been measured after the pulse has passed the specimen and is affected by the failure process and the geometry of the specimen. The response measured in the experiments is influenced by structural effects such as the geometry of the specimen and the stiffness of the experimental set-up. For this reason material parameters which determine the post-peak response cannot be derived directly from the experiment. However, the combination of experimental and numerical analyses makes it possible to separate the structural from the material response, provided that a mathematically sound material model is used and that the geometry and boundary conditions have been modeled correctly.

For the numerical modeling of the specimen and the Split–Hopkinson bar we assume a plane-stress condition, thus neglecting possible three-dimensional effects. The upper and lower bar of the Split–Hopkinson bar are very long to avoid reflections of the stress waves, which would result in a disturbed response. In the numerical simulation the test rig can therefore not be omitted, but must be modeled for a proper calculation of the response without undesirable reflections. However, the element size in the numerical modeling of the test rig is limited to the length traversed in one time step by the longitudinal elastic wave. Use of a larger element size would disturb the shape of the impact loading wave. A
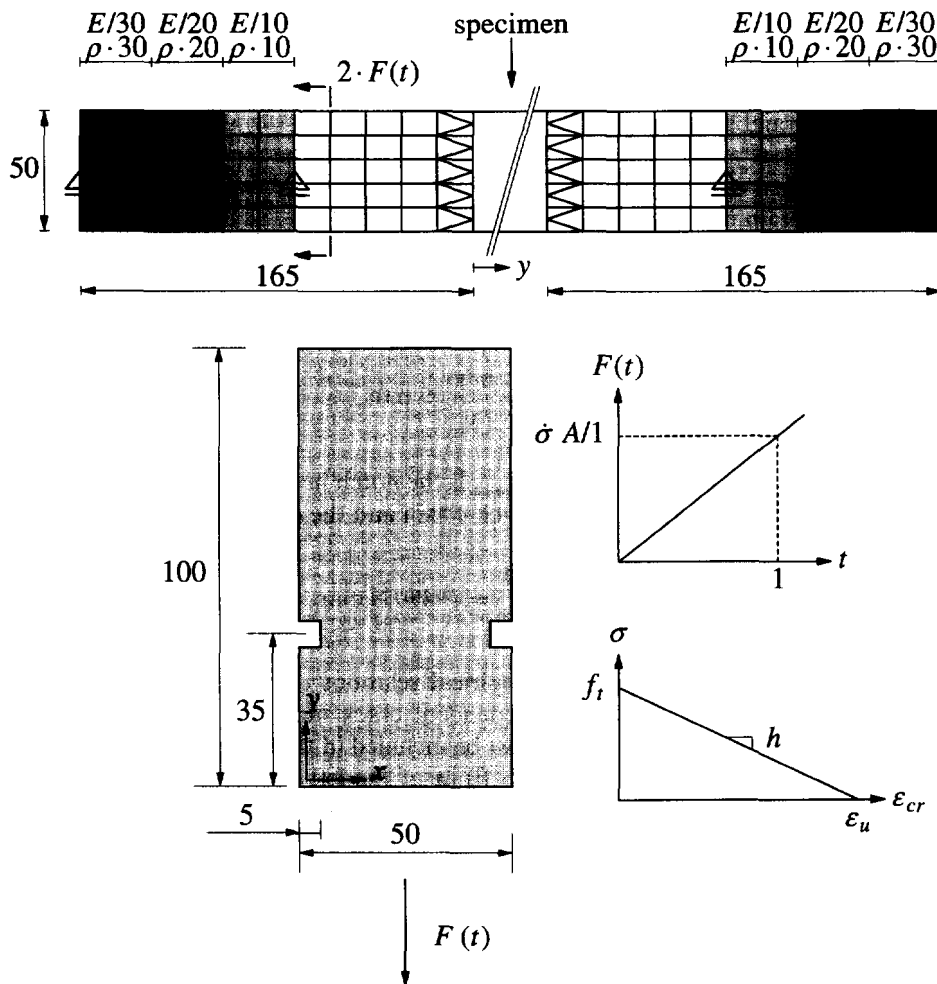
Fig. 3. Impact test on a double-notched specimen. Top: finite element model of test rig. Bottom: geometry, loading and material data for specimen.

straightforward discretization of the total Split-Hopkinson bar is therefore too expensive. A configuration with fewer elements can be obtained if we make use of the acoustic impedance,

$$Z = A\sqrt{\rho E},$$ (9)

of the material, in which A is the cross-sectional area of the adapter. If Z is kept constant, no reflections occur at an interface of materials with different properties. In this way the wave speed can be slowed down by an increase of the density ρ and a decrease of Young's modulus E. Using this technique several zones are applied to gradually slow down the wave speed. The numerical model with these artificial damping zones is given in Fig. 3. Since the numerical model of the test rig is not complete we have different boundary conditions from the conditions in the test. The upper and lower bar of the test rig have been modeled with quadrilateral eight-noded elements with a four-point Gauss integration and with triangular six-noded elements with a three-point Gauss integration. To avoid reflections at the transition of the specimen and the test rig the same material parameters are chosen for the test rig as for the specimen. For the specimen three finite element discretizations have been used. For the different meshes we use one, two and four rows of elements in the notched section, respectively. The elements are eight-noded quadrilaterals with a nine-point Gauss integration. The specimen geometry is width 50 mm, height 100 mm and depth 80 mm and the notch is 5 × 6 mm (Fig. 3). The applied load is doubled because half of the load propagates to the specimen as a tensile wave and the other half propagates to the boundary

elements as a pressure wave and is taken as $\dot{\sigma}A = 34.56 \times 10^6$ N s^{-1} with A the net cross-section area 40×80 mm. For the plain concrete we have the Young's modulus $E_c = 40,700$ N mm^{-2}, Poisson's ratio $v = 0.2$ and density $\rho = 2350$ kg m^{-3}. The inelastic parameters are derived by a straightforward translation of experimental data, which is not a proper method when we deal with localization phenomena as discussed before. In an inverse procedure this analysis can be seen as a first iteration. Here it is done to show the spurious solution that we obtain if we use a standard crack model. A simple linear strain-softening model is used and in a classical way, using a homogenization technique, the ultimate crack strain ε_u was derived from the ultimate deformation measured in the experiment according to

$$\varepsilon_u = \frac{\delta_u}{d_{notch}} = \frac{0.06}{6} = 0.01, \tag{10}$$

in which ε_u is the ultimate crack strain and d_{notch} is the notch height. The constant softening modulus h was derived from the ultimate crack strain and the dynamic tensile strength f_t

$$h = -\frac{f_t}{\varepsilon_u} = -\frac{4.9}{0.01} = -490 \text{ N mm}^{-2}. \tag{11}$$

The dynamic value for f_t is taken from empirical relations derived in former programs (Zielinski, 1982). In contrast to the rate-dependent crack model for the standard crack model the increase of the tensile strength must be included in the softening function. In the numerical analyses a section of 5×6 mm in front of the left notch was given a material imperfection in the sense that the tensile strength was reduced by 20%. By inserting an imperfection the possibility is offered of computing an asymmetric component of the solution. For the standard crack model we use f_t and ε_u, while for the rate-dependent crack model the additional parameter the viscosity m and, implicitly the length scale l, must be chosen.

The semi-discrete equations of motion have been solved with a Newmark time integration scheme using the updates.

$$\dot{\mathbf{a}}^{t+\Delta t} = \dot{\mathbf{a}}^t + [(1-\gamma)\ddot{\mathbf{a}}^t + \gamma\ddot{\mathbf{a}}^{t+\Delta t}]\,\Delta t \tag{12}$$

and

$$\mathbf{a}^{t+\Delta t} = \mathbf{a}^t + \dot{\mathbf{a}}^t\Delta t + [(\tfrac{1}{2}-\beta)\ddot{\mathbf{a}}^t + \beta\ddot{\mathbf{a}}^{t+\Delta t}]\,\Delta t^2, \tag{13}$$

in which $\ddot{\mathbf{a}}$, $\dot{\mathbf{a}}$ and $\mathbf{a}$ are the nodal accelerations, velocities and displacements, respectively. The integration constants are taken equal to $\beta = 1/4$ and $\gamma = 1/2$ corresponding to an average acceleration scheme. The time step in all analyses $\Delta t = 1 \times 10^{-6}$ s and a consistent mass matrix has been used. The Newmark scheme is used in combination with a full Newton–Raphson procedure to solve the nonlinear algebraic set of equations.

The results of the analyses with the standard crack model show the problem of mesh dependence as a consequence of the difficulty of the rate boundary value problem. Cracks start to propagate in one row of elements from the two notches to the center of the specimen. In Fig. 4 it is shown that the deformation (plotted with a multiplication factor equal to 500) localizes in one single row of integration points for each of the three meshes. A second problem becomes apparent which is caused by the complex nature of the problem, namely the mesh alignment of the results, i.e. the cracks or the localization of deformation have a preferential direction of propagation which is aligned with the mesh lines. For mesh 3 we observe a clear spurious deformation pattern with the localization concentrated in a single band of elements which generally follows the mesh lines and occasionally jumps from one row to the next and back without any physical motivation. The relation between fineness of mesh and post-peak response for the standard crack model is demonstrated in Fig. 5. It

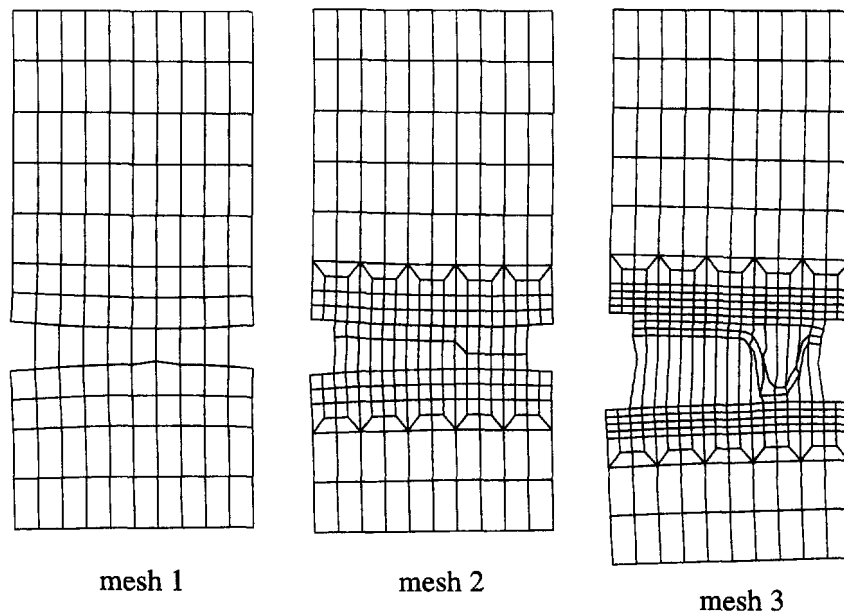mesh 1   mesh 2

mesh 3

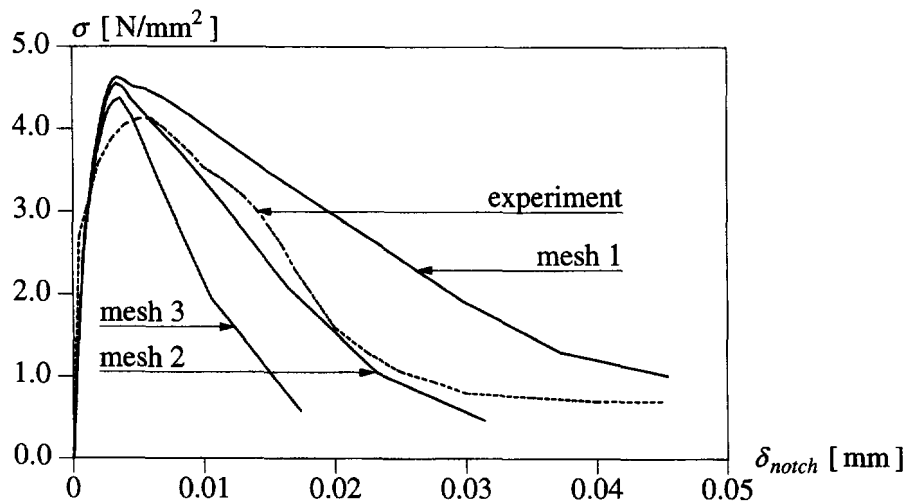Fig. 4. Displacement patterns at $t = 0.50 \times 10^{-3}$ s.

Fig. 5. Stress–deformation curve inside the fracture zone.

shows a stress–deformation curve, in which δ_{notch} represents the mean deformation over the left and the right notch and σ represents the vertical stress at the top of the specimen. A comparison can be made with experimental data (Weerheijm, 1992). The area under the curve is not an objective measure for the fracture energy. Mesh dependence starts already in the pre-peak regime, when the cracks propagate from the notch to the center of the specimen. This results in a lower peak stress for the finest mesh.

The same test has also been analyzed using the G_f-type crack model. The model guarantees a mesh-objective fracture energy dissipation for this problem with one failure plane, but the observation that localization zones are biased by the discretization and tend to propagate along mesh lines still holds (see Glynn, 1995).

For the analysis with the rate-dependent crack model we apply a slight modification of the parameter set. For the standard crack model the increase of tensile strength due to dynamic effects must be incorporated entirely in the strain-softening function, whereas in the rate-dependent crack model strain-softening can occur before the ultimate stress is reached. Already in the pre-peak regime we model at a constitutive level some damage through strain-softening while viscous effects cause the further increase of the stress. For

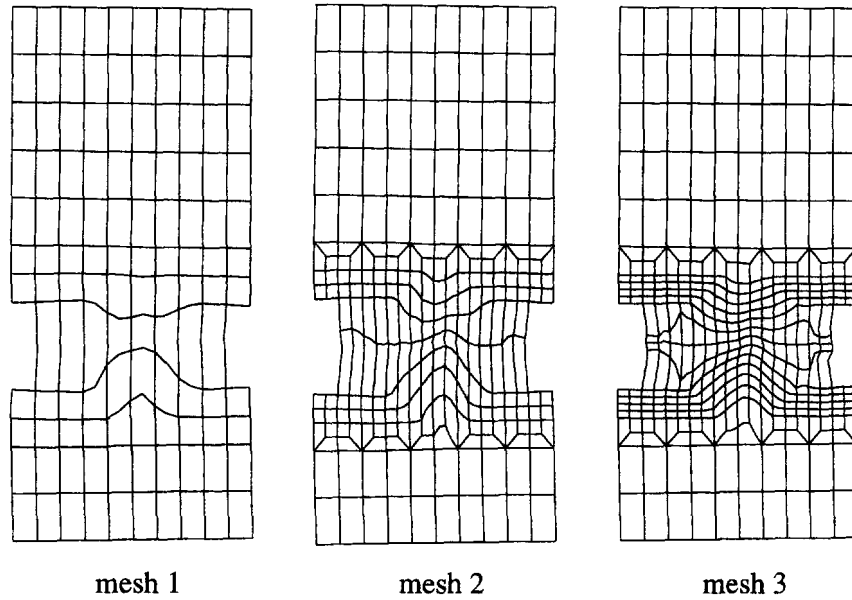mesh 1   mesh 2   mesh 3

Fig. 6. Incremental displacement pattern at $t = 0.45 \times 10^{-3}$ s.

this reason a redistribution of stresses is possible already in the pre-peak regime. In this analysis we assume that the stress at which strain softening starts is 80% of the dynamic tensile strength of the concrete, 4.9 N mm^{-2}, yielding $f_t = 3.92$ N mm^{-2}. In experiments it is observed that at this stress level micro-cracks start to develop. Furthermore, we take the strain-softening modulus $h = -2500$ N mm^{-2} and the viscosity $m = 0.1$ Ns mm^{-2}. In combination with the used parameter set this results in a length scale parameter $l = 20.5$ mm [eqn (4)].

The results in Figs 6–9 show markedly the effect of viscous regularization. At the notches the very local stress concentrations keep the band small, but the width of the localization band increases when the crack propagates to the center of the specimen. The patterns of the incremental displacements in Fig. 6 show the independence of the fineness and the directional bias of the mesh. The cracks branch off and the deformation band becomes wider, independent of the direction of the grid lines. The development of the
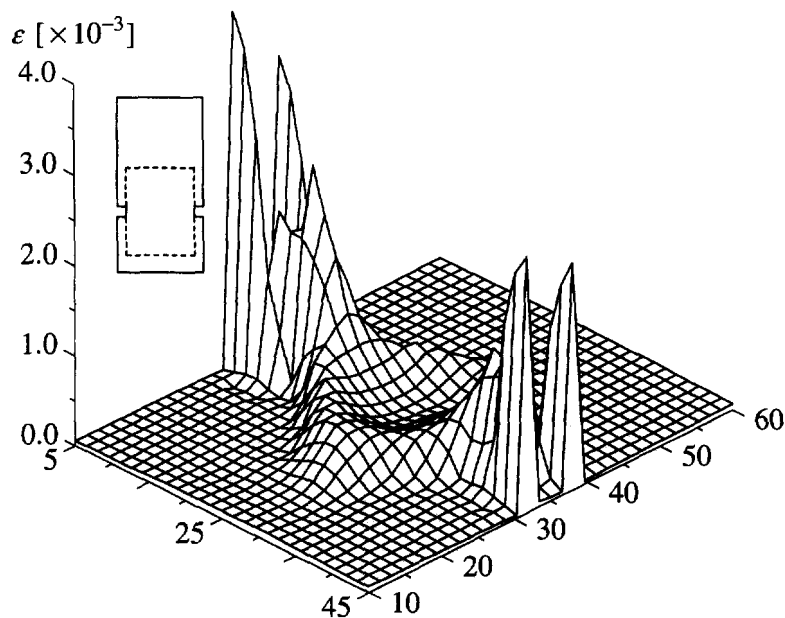

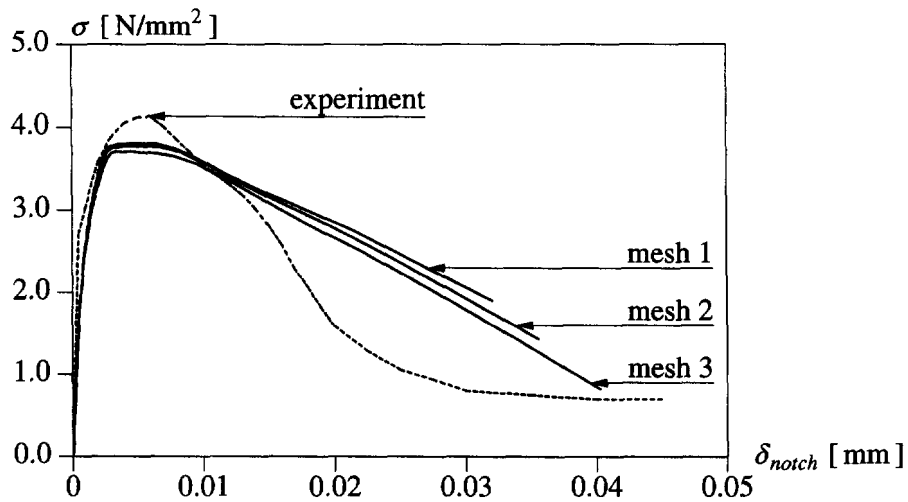Fig. 7. Development of the localization zone (axial strains—mesh 3—$t = 0.45 \times 10^{-3}$ s).
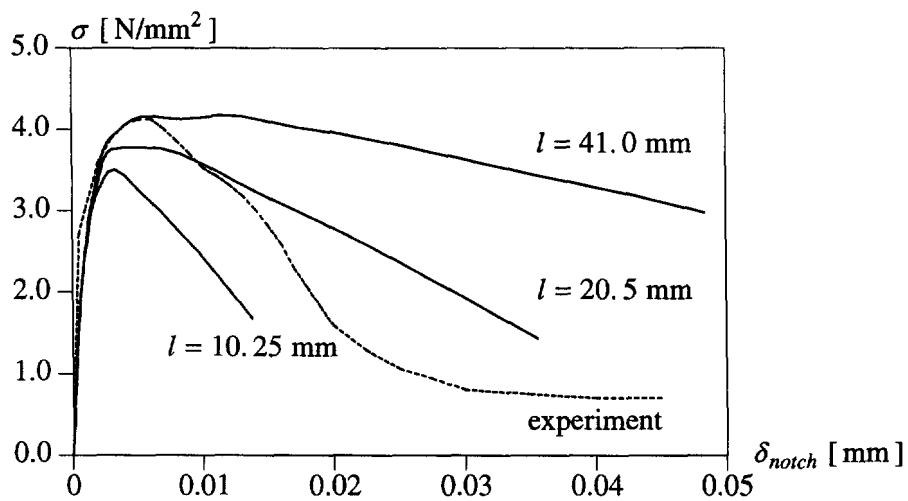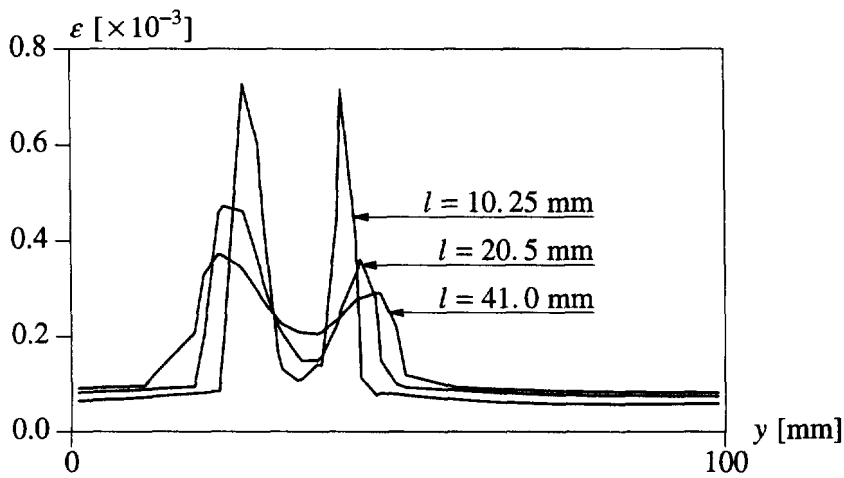
Fig. 8. Stress–deformation curve inside the fracture zone.

Fig. 9. Variation of the length scale parameter. Top: axial strain ($l = 10.25$ mm, $t = 0.41 \times 10^{-3}$ s, $l = 20.5$ mm, $t = 0.45 \cdot 10^{-3}$ s, $l = 41.0$ mm, $t = 0.48 \cdot 10^{-3}$ s). Bottom: stress-deformation curve inside the fracture zone.

fracture process zone is shown in Fig. 7 for the axial strains in the area between the notches. Cracking starts at the upper and lower corners of the notches. Both cracks at the left notch first join and at a later stage split up into two separate localization bands. Hence there remains an almost unstretched zone in the center of the specimen. The same crack propagation process occurs at the right notch. Again, the numerical results have been compared with the experimental data (Weerheijm, 1992). The stress–deformation curves of the numerical analyses as well as those of the experiment have been plotted in Fig. 8. We observe not only mesh independence, but also a reasonable agreement between numerical analyses and experiment. The calculated maximum tensile stress is slightly smaller and the application of a linear strain-softening model prevents the proper simulation of a nonlinear softening branch, which has been measured in the experiment. Finally, the effect of a variation of the length scale parameter l has been examined through varying the viscosity m. In Fig. 9 the axial strains in a cross-section ($x = 25$ mm) show the dependence of the localization zone on l. An increase of l by a factor of 2 provides a wider and smoother localization zone, whereas a division of l by 2 yields sharper peaks for the strains in a smaller localization zone. In the stress–deformation curve in Fig. 9 a smaller value for l leads to a steeper drop in the curve and a more brittle behavior, whereas an increase of l yields a more ductile response, although the maximum stress is predicted more accurately. Hence, l is a parameter which has an influence similar to that of the fracture energy G_f.

Now the role of the imperfection adjacent to the left notch, which has been applied in order to trigger an asymmetric failure mode, will be discussed. The rotation during failure which is observed in the test is found to be less pronounced in the numerical simulations. The analysis with $l = 41.0$ mm shows a purely symmetric response, $l = 20.5$ mm leads to a slight rotation of the specimen and only $l = 10.25$ mm offers the possibility of simulating rotation of the crack plane. However, the latter analysis gives a worse prediction of the global response as observed in Fig. 9. A remarkable result is that in the experiment as well as in the numerical simulation ($l = 10.25$ mm) the entire rotation occurs in the pre-peak regime. Rotation starts when the first cracks appear at the left notch and reaches its maximum when the crack pattern is complete and the ultimate stress is reached. As discussed before the response is influenced not only by material behavior, but also by structural effects. It is plausible that the test rig has an influence on at least a part of the rotation of the specimen. In the numerical simulation the test rig differs from the real configuration, as has been discussed above, which can be a cause of the poor prediction of the rotation of the specimen. A second point of consideration is the plane-stress modeling of an experiment in which three-dimensional effects are present. This can also contribute to an asymmetric response. A third possible cause for the discrepancy is the linear softening branch that has been utilized.

5. REINFORCED CONCRETE—PREDICTION OF CRACK SPACING

We now consider a reinforcing bar which is loaded at two sides by impact loads $F(t)$. The loading is such that cracking is initiated when the two loading waves meet in the center of the bar while the response of the steel bar remains elastic. A relatively long bar has been used to prevent waves reflecting at the two ends of the bar before the primary crack pattern has developed. The data set for the reinforcing bar problem is as follows (symbols are explained in Fig. 10). The bar geometry is length $L = 4000$ mm, cross-section $A = 100 \times 100$ mm^2 and a $\varnothing 20$ reinforcement bar. The applied loading is distributed over the cross-section such that the interactive forces at both ends are zero, i.e. $F_0 = 18.3$ kN (15.0 kN on the concrete and 3.3 kN on the steel bar) and $t_d = 0.00005$ s. For the concrete we have a Young's modulus $E_c = 30{,}000$ N mm^{-2}, Poisson's ratio $v = 0.2$, density $\rho = 2400$ kg m^{-3}, tensile strength $f_t = 2.0$ N mm^{-2} and ultimate strain $\varepsilon_u = 0.001$. For the G_f-type crack model the additional parameter is the finite element size, while for the gradient crack model used here the gradient constant $\bar{c}$, and implicitly the length scale l must be defined. The algorithmic aspects of the mixed finite element formulation for the gradient model with reduced integration are given in Pamin (1994). The constitutive equation for the reinforcement reads: $E_s = 210{,}000$ N mm^{-2}, $\rho = 7800$ kg m^{-3} and $f_{sy} = 500$ N mm^{-2} and for the
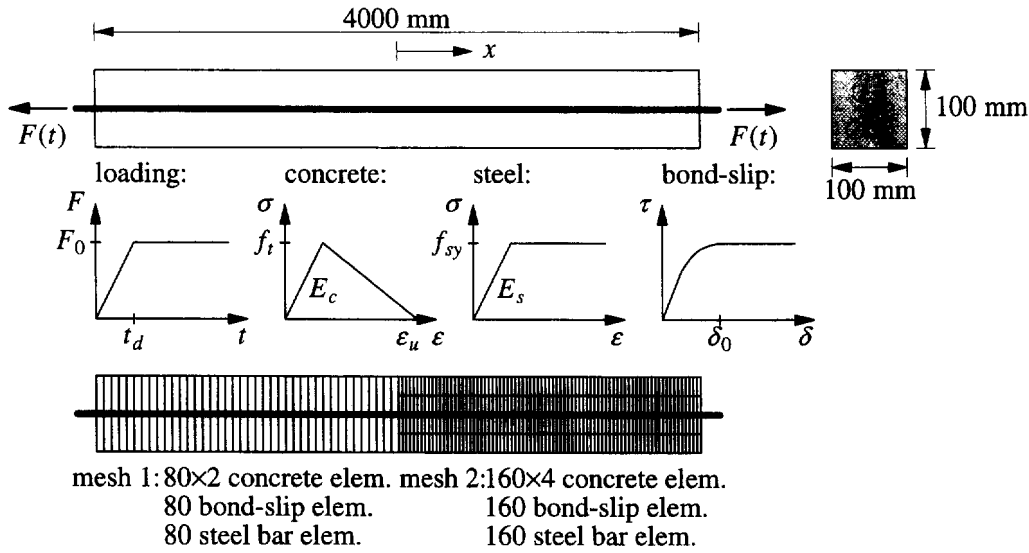
Fig. 10. Reinforcing bar.

bond–slip characteristic $a = 2.0$ N mm^{-2} and $\delta_0 = 0.06$ mm [cf. eqns (7)–(8)]. Again, a Newmark time integration scheme has been used with $\Delta t = 2.5 \times 10^{-6}$ s, $\beta = 1/4$, $\gamma = 1/2$ and the mass consistently distributed. Two different meshes have been used, see Fig. 10.

5.1. Perfect bond

Perfect bond can be established by omitting the interface elements from the finite element geometry in Fig. 1. If the response of the steel remains elastic, perfect redistribution of stresses in the bar is obtained. The crack concept has been studied for the perfect bond case and the results are shown in Figs 11–13. In Fig. 11 the strains in the concrete are given for the standard crack model with mesh 1 and with mesh 2. The classical mesh-sensivity problem for the crack width also plays a role for softening materials with reinforcement, since all deformations per primary crack occur in one vertical row of finite elements. The number of cracks computed for mesh 1 decreases considerably when using mesh 2. Consequently, the bar discretized with a finer mesh behaves more brittle (less energy per primary crack is consumed) which reduces the number of cracks. Since the crack spacing is not computed correctly the amount of energy that is consumed in the bar is arbitrary.

For the gradient model the results are different. Taking the length scale parameter $l = 10$ mm gives a dense pattern of primary cracks (see Fig. 12). The results are no longer arbitrary, i.e. for the two meshes we obtain similar results, although mesh 1 is still slightly too coarse to reproduce this crack pattern. For this case, i.e. without the incorporation of bond–slip, the length scale parameter l sets a value for the crack spacing $l_s \approx 92$ mm. For
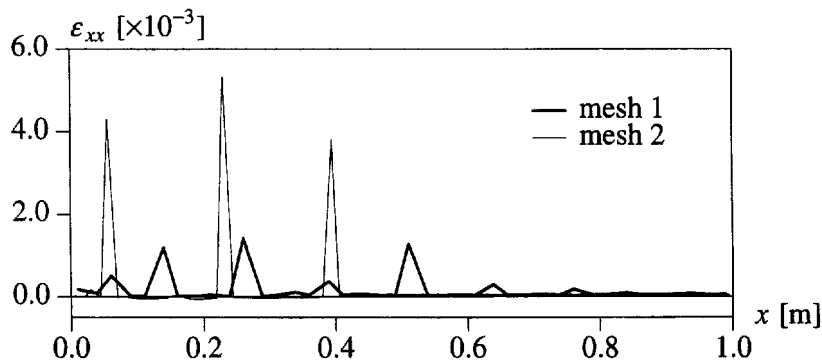

Fig. 11. Standard crack model—perfect bond—mesh 1 and 2—$t = 0.0015$ s. Arbitrary locations of primary cracks.
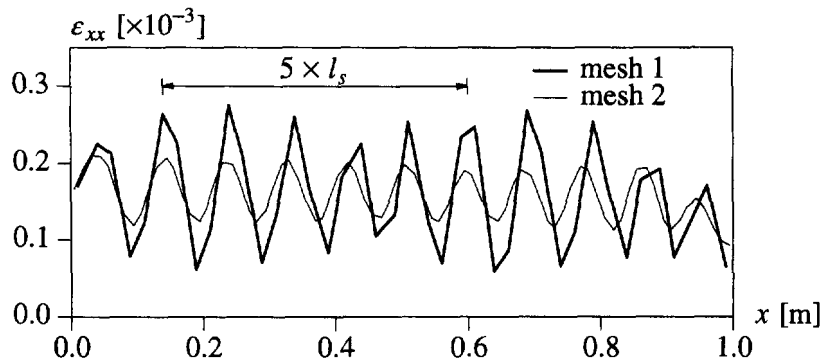
Fig. 12. Gradient crack model with $l = 10$ mm—perfect bond—mesh 1 and 2. Crack spacing l_s at $t = 0.0015$ s.
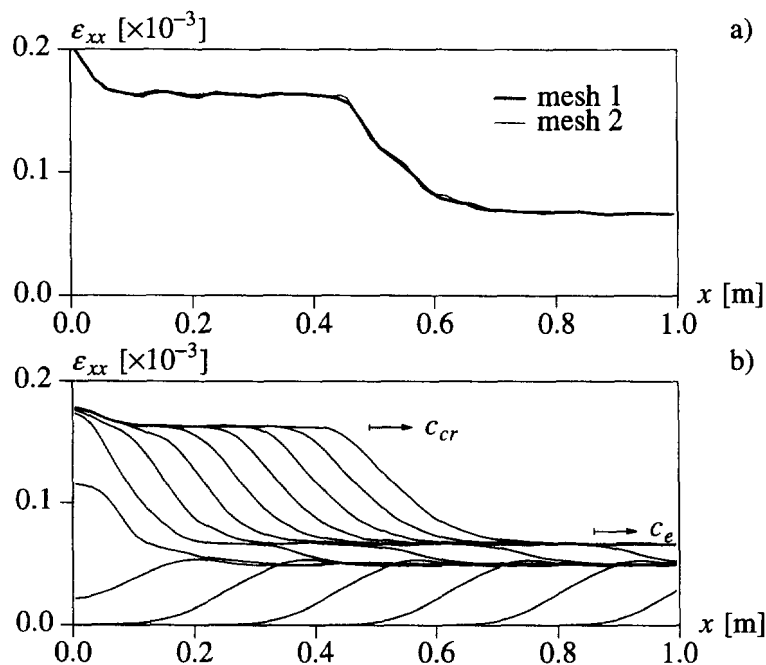

Fig. 13. Gradient crack model with $l = 20$ mm—perfect bond. (a) Uniform distribution of strain in concrete at $t = 0.001$ s; (b) stroboscopic evolution of strain in reinforcement $(0 < t < 0.001$ s).

an analysis with a length scale $l = 20$ mm the results are given in Fig. 13a. For this analysis the perfect redistribution of the stress through the perfect bond behavior results in a uniform distribution of crack strains over the bar. After the two waves have met in the center of the bar the elastic wave is split up into an elastic part $(f_t - F_0/A)$ which approximately propagates with the bar velocity $c_e = \sqrt{E/\rho}$ and an inelastic part that causes cracking which propagates with speed c_{cr}. As shown in Fig. 13b the strains in the reinforcement, which remain elastic, are the same as the total strains (sum of elastic and crack strain) in the concrete. It can be said that there is a certain threshold in the length scale parameter above which a uniform distribution of crack strain is found.

5.2. Bond–slip

For the proper calculation of the crack spacing and the crack width the inclusion of bond–slip is crucial. To demonstrate the character of the solution for an analysis with the standard crack model Fig. 14 shows the plots for the strains in the concrete (a) and the steel (b), the shear deformation in the interface (c) and the axial displacements (d). After the two waves have met a first primary crack appears. When the stress wave propagates further a second and a third primary crack occur. At the locations of primary cracks a
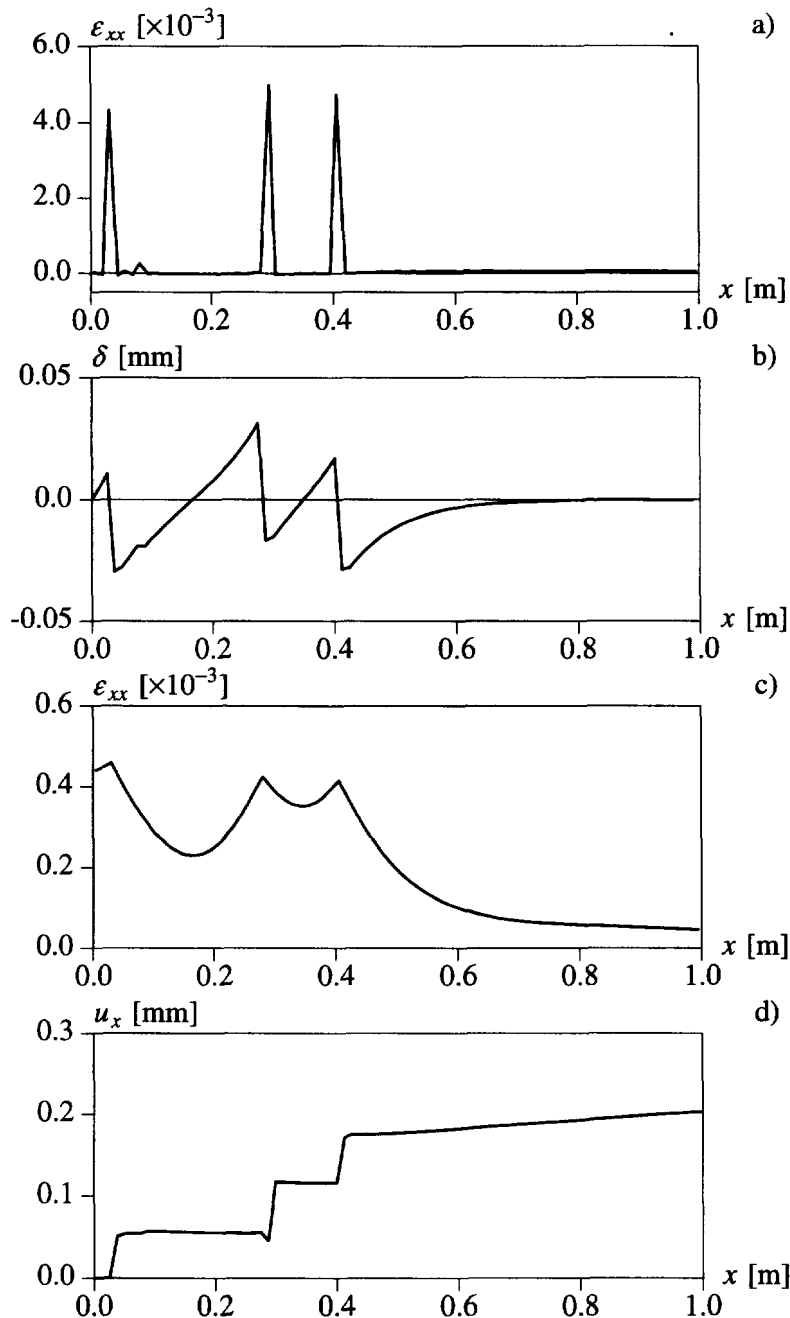
Fig. 14. Standard crack model—bond-slip—mesh 2—$t = 0.0015$ s. (a) Strain in concrete; (b) shear deformation in interface; (c) strain in steel and (d) axial displacements.

steep gradient in slip in the interface element takes place. Although the response of the steel is elastic the peaks in the strain profile are clear. For the standard crack model as well as for the G_f-type crack model the dependence of the crack spacing on the spatial discretization (mesh size) and the time integration scheme (Newmark—average acceleration vs Newmark—damped) have been studied and the results are given in Fig. 15. For these analyses a primary crack occurs in one vertical row of finite elements, and the spacing between the cracks is influenced by the finite element size and the time integration procedure. The latter observation is shown for different Newmark schemes, but a variation of time step or a lumping of the mass lead to similar spurious results. The mesh dependence with respect to the crack spacing cannot be repaired by using a G_f-type crack model and for this reason global mesh-objectivity for the strain energy consumption (as obtained in plain concrete
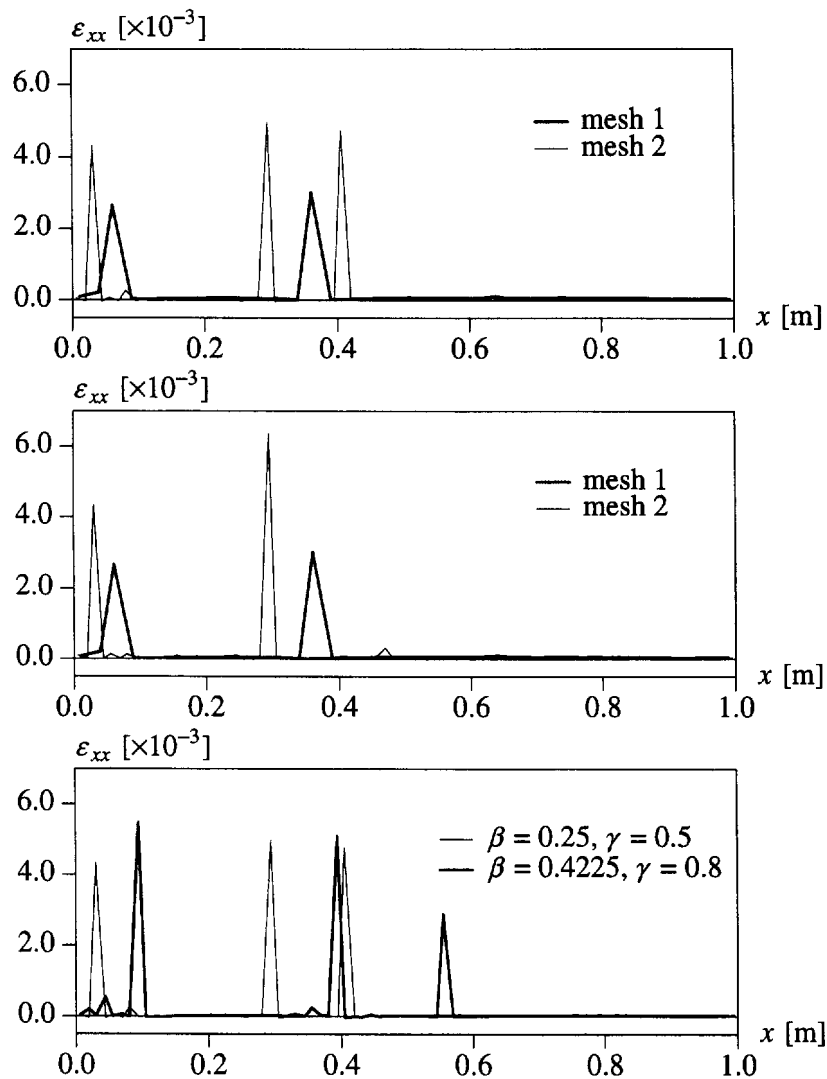
Fig. 15. Comparison of crack models—bond–slip—$t = 0.0015$ s. Top: standard crack model—mesh 1 and mesh 2. Center: G_f-type crack model—mesh 1 and mesh 2. Bottom: variation of time integration scheme—mesh 2.

analyses with this model) is not achieved. Although the amount of energy consumed per crack is roughly the same for both meshes, the location of the primary cracks and the crack spacing, which is related to the number of cracks, is arbitrary.

For the gradient model with a length scale $l = 20$ mm the in-objectivity in crack width and crack spacing is removed completely. The two meshes give the same results for the response in the concrete, the interface and the steel (see Fig. 16). The distance between the cracks is rather constant ($l_s \approx 190$ mm). If we match the value for the crack spacing l_s with the crack spacing measured in experiments, the length scale parameter that is needed in the computation can be determined. Consequently, the gradient parameter $\bar{c}$, which is a function of the length scale parameter, follows from the crack spacing observed in tests. The influence of the length scale parameter l on the crack spacing l_s has been analyzed in Fig. 17. It is clear that the crack spacing is proportional to the length scale. A remarkable result is obtained for smaller length scales (see Fig. 18). From the two pictures with a stroboscopic evolution of the crack strain it is observed that, first a pattern with cracks at regular distances occurs, while upon further loading the crack spacing is reduced by a factor of two. Only the localized deformation of every other primary crack further evolves.
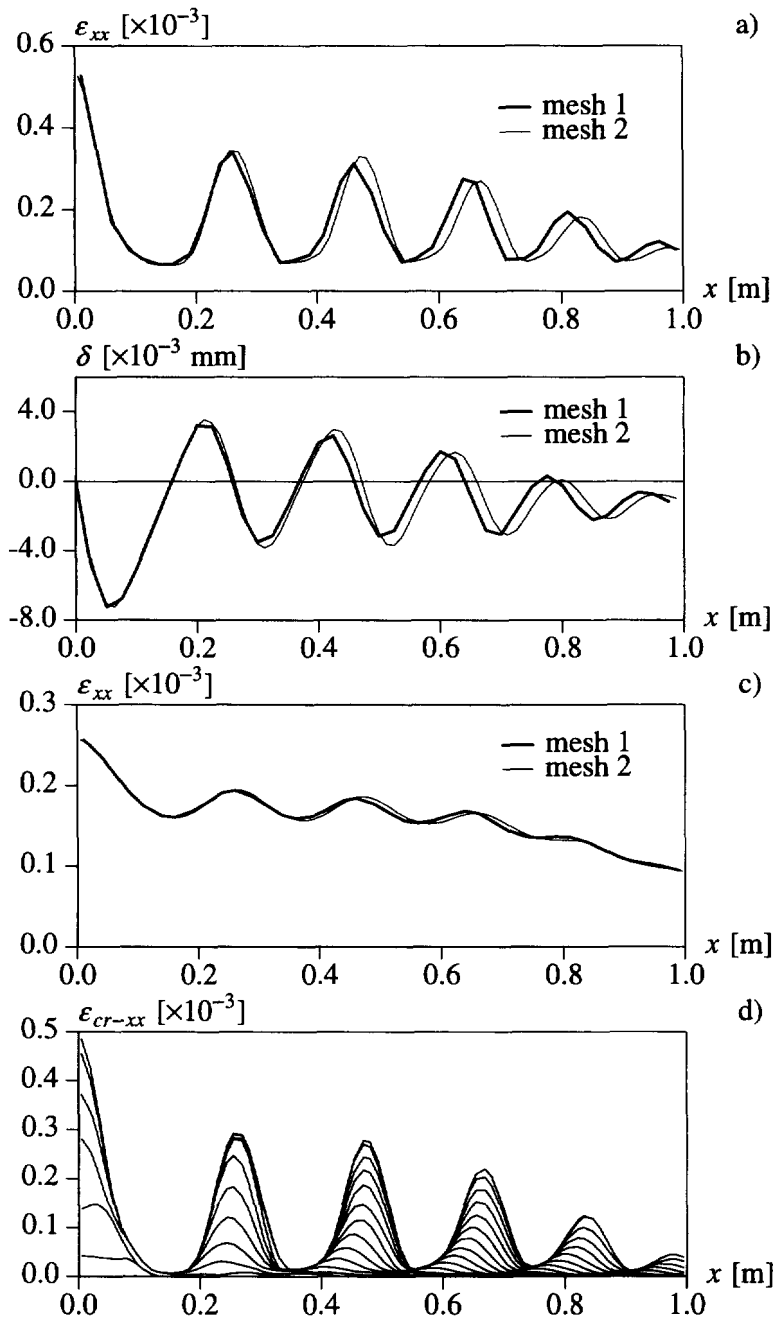
Fig. 16. Gradient crack model with $l = 20$ mm—bond–slip—$t = 0.0015$ s. (a) Strain in concrete; (b) shear deformation in interface; (c) strain in steel and (d) stroboscopic development of crack strains.

Finally, the influence of the bond–slip characteristic on the crack spacing has been investigated. Three shear traction–slip curves have been considered. Compared to the reference curve, the level of deformation, $\delta = \delta_0$, and the level of shear traction at which perfect slip occurs, $\tau = 1.9a$, have been increased by a factor of 2 and 1.5, respectively (see Fig. 19). The curves show the crucial role that the bond–slip behavior plays in the analysis. A stiffer bond–slip characteristic decreases the distance between the primary cracks while a softer bond–slip relation increases the value for the crack spacing. Again, perfect bond between concrete and reinforcement completely smooths out the inelastic deformations and a crack spacing cannot be observed (at least not with this length scale parameter).
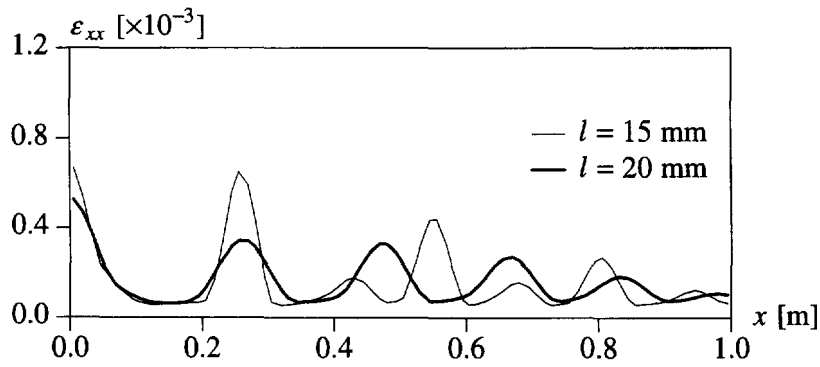
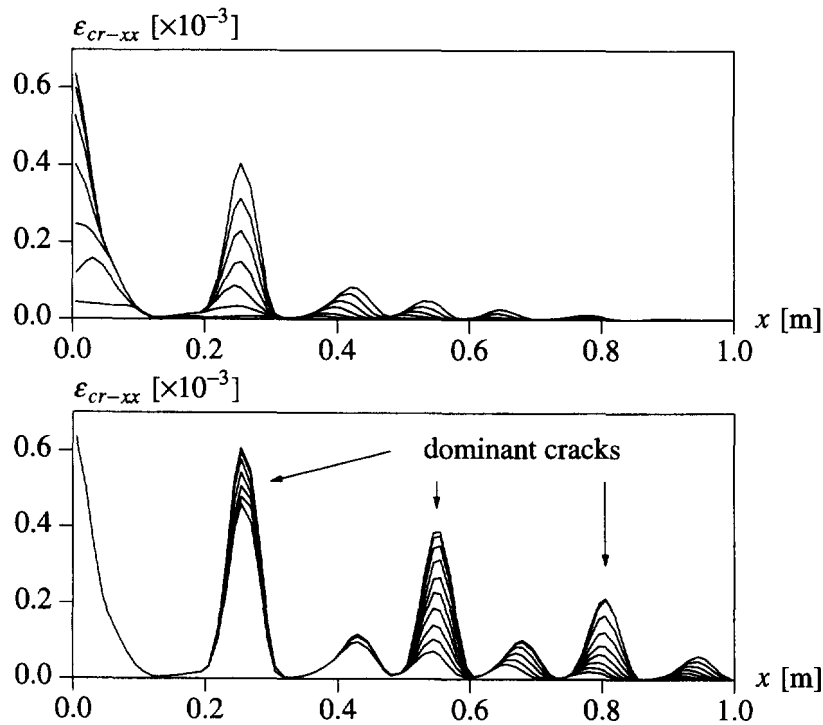Fig. 17. Gradient crack model—mesh 2—$t = 0.0015$ s. Variation of the length scale parameter.

Fig. 18. Gradient crack model with $l = 15$ mm—mesh 2—shift in primary crack pattern. Top:
$0 < t < 0.001$ s. Bottom: $0.001 < t < 0.0015$ s.

6. CONCLUDING REMARKS

The width of a single crack in plain concrete and the spacing of primary cracks in reinforced concrete have been studied. Attention is focused on the influence of the crack concept on the crack spacing. A comparison has been made between the standard crack model, the fracture energy-type crack model, the rate-dependent crack model and the gradient crack model. By using the standard crack model mesh sensitivity is obtained for the width of a single crack and for the spacing between cracks in reinforced elements. Although a fracture energy-type model prevents the energy release per primary crack from going to zero upon mesh refinement, the results for the crack spacing remain arbitrary. Both spatial and time discretization influence the value for the crack spacing when we use a standard crack model or a fracture energy-type crack model. The strain-rate dependent crack model and the strain-gradient model provide satisfactory results through the introduction of a length scale parameter. Mesh sensitivity with respect to the crack width in plain concrete and the crack spacing in reinforced concrete can be removed. The additional
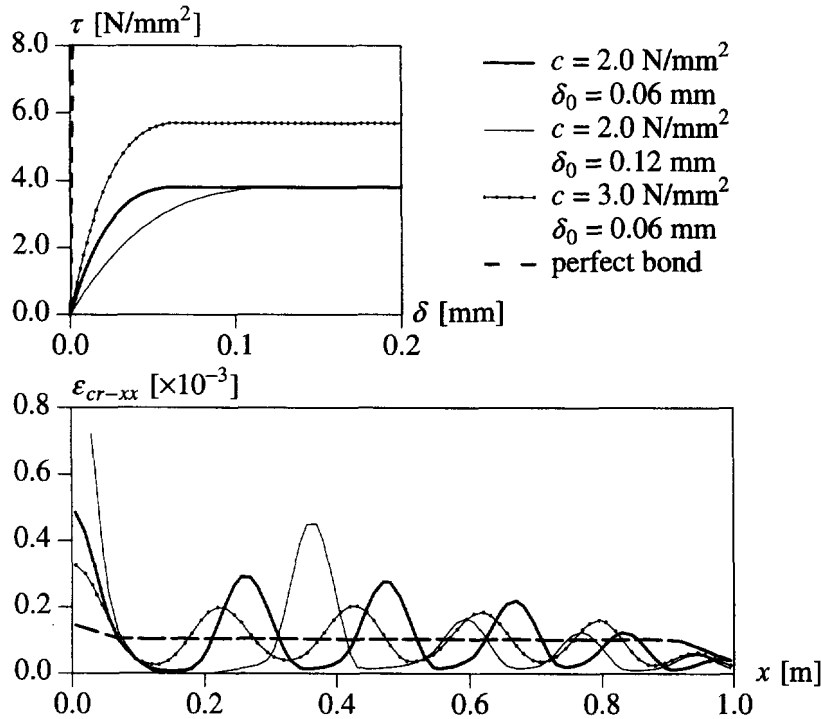
Fig. 19. Gradient crack model with $l = 20$ mm—mesh 2. Influence of the bond–slip characteristic.

parameter in the gradient model can be coupled to the crack spacing measured in experiments. Furthermore, the crucial role of the bond–slip characteristic in predicting crack spacing in reinforced elements is highlighted.

REFERENCES

Aifantis, E. C. (1984). On the microstructural origin of certain inelastic models. *J. Engng Mater. Technol.* **106**, 326–334.

Bažant, Z. P. and Oh, B. (1983). Crack band theory for fracture of concrete. *Mater. Struct.* **16**, 155–177.

Borst, R. de and Mühlhaus, H.-B. (1992). Gradient-dependent plasticity: formulation and algorithmic aspects. *Int. J. Numer. Meth. Engng* **35**, 521–539.

Dörr, K. (1980). Ein Beitrag zur Berechnung von Stahlbetonscheiben unter besonderer Berücksichtiging des Verbundverhaltens. Dissertation, Universität Darmstadt, Darmstadt.

Feenstra, P.H. (1993). Computational aspects of biaxial stress in plain and reinforced concrete. Dissertation, Delft University of Technology, Delft.

Glynn, J.L. (1995). A combined experimental-numerical study of notched concrete specimens under static and dynamic loading. TU-Delft report no. 03-21-0-31-31, Delft University of Technology, Delft.

Körmeling, H.A. (1986). Strain rate and temperature behaviour of steel fibre concrete in tension. Dissertation, Delft University of Technology, Delft.

Larsson, R. (1990). Numerical simulation of plastic localization. Dissertation, Chalmers University of Technology, Göteborg.

Lasry, D. and Belytschko, T. (1988). Localization limiters in transient problems. *Int. J. Solids Struct.* **24**, 581–597.

Loret, B. and Prévost, J. H. (1990). Dynamic strain localization in elasto-(visco-)plastic solids, Part 1. General formulation and one-dimensional examples. *Comp. Meth. Appl. Mech. Engng* **83**, 247–273.

Mülhaus, H.-B. and Aifantis, E. C. (1991). A variational principle for gradient plasticity. *Int. J. Solids Struct.* **28**, 845–858.

Needleman, A. (1988). Material rate dependence and mesh sensitivity on localization problems. *Comp. Meth. Appl. Mech. Engng* **67**, 69–86.

Pamin, J. (1994). Gradient-dependent plasticity in numerical simulation of localization phenomena. Dissertation, Delft University of Technology, Delft.

Pietruszczak, S. and Mróz, Z. (1981). Finite element analysis of deformation of strain softening materials. *Int. J. Numer. Meth. Engng* **17**, 327–334.

Rots, J. G. (1988). Computational modeling of concrete fracture. Dissertation, Delft University of Technology, Delft.

Simo, J. C. (1994). A new methodology for the numerical description of strain softening in inelastic solids. Contract report CR 95.002. Naval Facilities Engineering Service Center, California.

Simo, J. C., Oliver, J. and Armero, F. (1993). An analysis of strong discontinuities induced by softening solutions in rate-independent solids. *J. Comput. Mech.* **12**, 277–296.

Sluys, L. J. (1992). Wave propagation, localisation and dispersion in softening solids. Dissertation, Delft University of Technology, Delft.

Sluys, L. J. and Borst, R. de (1992). Wave propagation and localization in a rate-dependent cracked medium— model formulation and one-dimensional examples. *In. J. Solids Struct.* **29**, 2945–2958.

Sluys, L. J., Cauvern, M. and Borst, R. de. (1995). Discretization influence in strain-softening problems. *Engng Comput.* **12**, 209–228.

Weerheijm, J. (1992). Concrete under impact tensile loading and lateral compression. Dissertation, Delft University of Technology, Delft.

Willam, K. (1984). Experimental and computational aspects of concrete fracture. In *Proc. Int. Conf. on Computer Aided Analysis and Design of Concrete Structures* (Edited by F. Damjanić *et al.*), pp. 33–70. Pineridge Press, Swansea.

Wu, F. H. and Freund, L. B. (1984). Deformation trapping due to thermoplastic instability in one-dimensional wave propagation. *J. Mech. Phys. Solids* **32**, 119–132.

Zielinski, A. J. (1982). Fracture of concrete and mortar under uniaxial impact tensile loading. Dissertation, Delft University of Technology, Delft.